# The structure of interfacial water on gold electrodes studied by x-ray absorption spectroscopy

Juan-Jesus Velasco-Velez *et al.*

*Science* **346**, 831 (2014);
DOI: 10.1126/science.1259437

3. C. Novo, A. M. Funston, A. K. Gooding, P. Mulvaney, *J. Am. Chem. Soc.* **131**, 14664–14666 (2009).
4. M. Nonnenmacher, M. P. O'Boyle, H. K. Wickramasinghe, *Appl. Phys. Lett.* **58**, 2921 (1991).
5. See supplementary materials on *Science* Online.
6. N. W. Ashcroft, N. D. Mermin, *Solid State Physics* (Harcourt, New York, 1976).
7. B. M. Askerov, S. Figarova, *Thermodynamics, Gibbs Method and Statistical Physics of Electron Gases* (Springer, New York, 2010).
8. M. G. Cerruti *et al.*, *Anal. Chem.* **78**, 3282–3288 (2006).
9. F. J. Blatt, P. A. Schroeder, C. F. Foiles, *Thermoelectric Power of Metals* (Plenum, New York, 1976).
10. M. W. Knight, H. Sobhani, P. Nordlander, N. J. Halas, *Science* **332**, 702–704 (2011).
11. N. Noginova, A. V. Yakim, J. Soimo, L. Gu, M. A. Noginov, *Phys. Rev. B* **84**, 035447 (2011).
12. W. L. Barnes, W. A. Murray, J. Dintinger, E. Devaux, T. W. Ebbesen, *Phys. Rev. Lett.* **92**, 107401 (2004).

**ACKNOWLEDGMENTS**

Supported by U.S. Department of Energy (DOE) Office of Science grant DE-FG02-07ER46405 (M.S. and H.A.A.), an NSF Graduate Research Fellowship (A.B.), and experimental facilities of the DOE "Light-Material Interactions in Energy Conversion" Energy Frontier Research Center grant DE-SC0001293. Work at AMOLF is part of the research program of the Foundation for Fundamental Research on Matter [which is financially supported by the Netherlands Organization for Scientific Research (NWO)] and by the European Research Council. The data are archived in the laboratory of H.A.A. and A.P. We thank E. Kosten, V. Brar, D. Callahan, M. Deceglie, A. Leenheer, J. Fakonas, R. van Roij, B. M. Mulder, and H. J. Bakker for helpful discussions.

**SUPPLEMENTARY MATERIALS**

www.sciencemag.org/content/346/6211/828/suppl/DC1
Materials and Methods
Supplementary Text
Figs. S1 to S9
References (*13*–*36*)

7 July 2014; accepted 16 October 2014
Published online 30 October 2014;
10.1126/science.1258405

INTERFACIAL WATER

# The structure of interfacial water on gold electrodes studied by x-ray absorption spectroscopy

**Juan-Jesus Velasco-Velez,[1] Cheng Hao Wu,[1,2] Tod A. Pascal,[3] Liwen F. Wan,[3] Jinghua Guo,[4,5] David Prendergast,[3] Miquel Salmeron[1,6]***

**The molecular structure of the electrical double layer determines the chemistry in all electrochemical processes. Using x-ray absorption spectroscopy (XAS), we probed the structure of water near gold electrodes and its bias dependence. Electron yield XAS detected at the gold electrode revealed that the interfacial water molecules have a different structure from those in the bulk. First principles calculations revealed that ~50% of the molecules lie flat on the surface with saturated hydrogen bonds and another substantial fraction with broken hydrogen bonds that do not contribute to the XAS spectrum because their core-excited states are delocalized by coupling with the gold substrate. At negative bias, the population of flat-lying molecules with broken hydrogen bonds increases, producing a spectrum similar to that of bulk water.**

Many important processes in electrochemical reactions, such as ion desolvation and charge transfer, occur in the so-called electrical double layer (EDL), also known as the Helmholtz layer (*1*). This layer, containing solvated ions and solvent molecules, is typically one to tens of nanometers thick, depending on solute concentration. An important characteristic of the EDL is the presence of a strong electric field perpendicular to the electrode surface that is believed to play a crucial role in determining its structure.

Among liquids, aqueous solutions play a vital role in chemistry, biology, and materials sciences. The strong dipole of the water molecule and its hydrogen-bonding network gives rise to distinctive properties, including the high boiling point and high specific heat capacity. It is expected therefore that perturbations of the local hydrogen bonding network near surfaces (*2*, *3*), together with strong electric fields, will influence the structure of the first molecular layers. Understanding the structure and dynamics of these interface layers is of fundamental importance and the object of our study.

A host of techniques have been used to study the EDL, including grazing incidence x-ray scattering (*4*) that provides crystallographic information and electronic density profiles, and vibration spectroscopies such as infrared (IR) and Raman (*5*, *6*), together with nonlinear second-order sum frequency generation (SFG), which have been used to study the vibrational nature of water molecules at interfaces (*7*). Using SFG at the glass-water interface at different pH values, it was concluded that protonation and deprotonation of oxide sites led to surface charges and electric fields that align the interfacial water molecules (*8*–*10*).

In contrast to these techniques, x-ray absorption spectroscopy (XAS) is element-specific and provides information about the electronic structure around the excited atom, which is sensitive to the local structure and chemical environment (*11*). XAS has been extensively used to study the structure of water by analyzing the oxygen K-edge spectra (*12*, *13*). XAS can be performed by collecting either photons or secondary electrons generated by the decay of the core holes created by the absorbed x-rays. The first detection mode, called total fluorescence yield (TFY) (*14*–*17*), is a bulk-sensitive technique, because the mean free path of soft x-rays is in the micrometer range. When collecting secondary electrons (the so-called total electron yield mode, TEY), the information is surface sensitive because of the short mean free path of electrons in condensed matter, on the order of nanometers for energies in the 100-eV range.

Our system consists of an electrochemical flow cell with an ultrathin $Si_3N_4$ membrane window (100 nm thick) that separates the liquid medium inside the cell from the high-vacuum environment of Beamline 8.0.1 in the Advanced Light Source at the Lawrence Berkeley National Laboratory (Fig. 1). The cell contains reference and counter electrodes for electrochemical experiments (*18*, *19*). The electrode under study is a ~20-nm Au film evaporated on the internal side of the $Si_3N_4$ membrane, in contact with a flowing aqueous 10 μM solution of NaCl. The film is continuous and fully covers the membrane surface, as shown by atomic force microscopy (AFM) imaging (fig. S1) (*20*). Gold was chosen because its inert nature makes it possible to explore a wide range of electrostatic potentials without inducing electrolysis or other electrochemical reactions that could alter the structure and composition of its surface. The lack of reactivity or ion adsorption was confirmed by the absence of peaks in the cyclic voltammetry curves (fig. S2) (*20*). Because the effective attenuation length of electrons with energy smaller than 530 eV (from the O K-edge excitation of water) is estimated to be between 5 and 10 Å in liquid water (*21*, *22*), the TEY signal should originate from the first two or three water layers. This was confirmed by theoretical calculations as discussed below.

Figure 2A shows the O K-edge XAS spectra of water at open circuit potential in TFY (curve a), and TEY detection modes (curves b and c). Curve a corresponds to the well-known oxygen K-edge spectrum of bulk water, which is divided into three regions: pre-edge region, around 535 eV (I); main edge region, around 537 eV (II); and post-edge region, around 540 eV (III). The pre-edge peak at 535 eV is characteristic of the liquid phase

[1]Materials Science Division, Lawrence Berkeley National Laboratory, Berkeley, CA 94720, USA. [2]Department of Chemistry, University of California, Berkeley, CA 94720, USA. [3]Joint Center for Energy Storage Research, The Molecular Foundry, Lawrence Berkeley National Laboratory, Berkeley, CA 94720, USA. [4]The Advanced Light Source, Lawrence Berkeley National Laboratory, Berkeley, CA 94720, USA. [5]Department of Chemistry and Biochemistry, University of California, Santa Cruz, CA 95064, USA. [6]Department of Materials Science and Engineering, University of California, Berkeley, CA 94720, USA.
***Corresponding author. E-mail: mbsalmeron@lbl.gov**

and originates from unsaturated donor (or dangling) hydrogen bonds (*11*, *12*, *23*). The main edge is similarly related to the population of molecules with unsaturated hydrogen bonds, while the post-edge region is associated with the fully saturated hydrogen bonding network. In bulk ice, the pre- and main-edge peaks are weak because all of the hydrogen atoms participate in hydrogen bonds. In liquid water, the pre-edge peak is relatively prominent, while the post-edge is weaker compared to ice (*12*, *24*). As can be seen in the TEY spectrum (curve b), no spectral feature is visible at 535 eV, which might be interpreted as indicative of a much lower concentration of broken hydrogen bonds at the gold-water interface compared to bulk water. In fact, as we shall see below, the contrary is true.

To gain insights into the measurements, we performed ab initio molecular dynamics (AIMD) simulations, to explore the interfacial structure of water near gold. We initiated our AIMD simulation from a pre-equilibrated box comprising 150 water molecules interfaced with six layers of gold atoms oriented to expose the (111) surface (Fig. 2B). To interpret the XAS measurements, we used a smaller model of the same interface and sampled five evenly spaced snapshots from the last 5 ps of AIMD trajectory. The calculation of the XAS was done with the constrained-occupancy density functional theory within the excited electron and core-hole (XCH) approach (*23*), which has been shown to be efficient in predicting the XAS of complex molecular systems (*25*, *26*).

Analysis of the AIMD trajectory revealed that 49% of the interfacial water molecules (i.e., water molecules within ~1 nm of the electrode) lie flat on the surface with both hydrogen bonds saturated, denoted as double-donor (DD) species (Fig. 3). These molecules are characterized by an XAS spectrum with no substantial pre-edge feature. Another 49% of the interfacial water molecules have one broken hydrogen bond, either parallel to the surface ($SD^{\parallel}$, 18%) or perpendicular ($SD^{\perp}$) with one hydrogen atom pointing toward the gold surface (31%). This population of broken H-bond molecules is substantially higher than the 22% found in bulk water.

We find that although the XAS of the $SD^{\parallel}$ molecules resembles that of SD molecules in the bulk, the XAS of the $SD^{\perp}$ molecules does not present a pre-edge feature. Similarly, water molecules with two dangling hydrogen bonds (ND species) are oriented with both hydrogen atoms pointing toward the gold surface and thus do not contribute to the pre-edge feature.

The suppression of the pre-edge of perpendicular water molecules with broken hydrogen bonds at the gold surface is a purely electronic effect. The core-excited state resulting from the absorption of a 535-eV x-ray photon is coupled to the gold band structure and delocalizes over the surrounding gold atoms (fig. S3) (*20*). This delocalization reduces the overlap of the core-excited electron with the 1s core hole at the excited oxygen atom, thereby reducing the transition probability and thus the peak intensity. Further, because the pre-edge peak arises from antibonding σ* states centered on the hydrogen atom and extending directionally along the OH bond vector (*27*), coupling to the gold depends strongly on the orientation of the water molecule and affects primarily the water molecules in the first layer. The water molecules with broken hydrogen bonds in the second layer also have a reduced pre-edge intensity, although the reduction is only about 30% that of the first layer. The net result is that the XAS obtained from sampling only the interfacial water molecules show a substantially reduced pre-edge feature. The good agreement with the TEY spectrum confirmed the high interfacial sensitivity of these measurements.

Our AIMD results, which show a large number of broken hydrogen bonds in the interfacial region, are consistent with previous simulations reporting substantial populations of interfacial water molecules oriented with hydrogen atoms pointing toward the Au surface (*28*, *29*). It is at odds, however, with conclusions based on studies of interfacial water at cryogenic temperatures, which may not represent the room-temperature liquid-solid

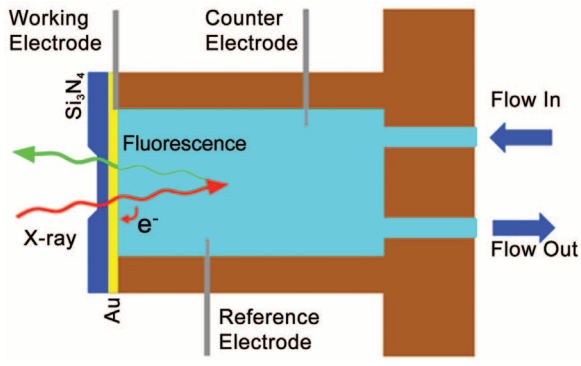


**Fig. 1. Schematic of the electrochemical cell.** A $Si_3N_4$ membrane (~100 nm thick) separates the liquid from the vacuum region of the synchrotron x-ray source. The gold electrode is a thin (20 nm) film evaporated on the back side of the membrane. Detection of x-ray absorption was done by collecting the fluorescence emission on the vacuum side and also by collecting secondary electrons at the gold electrode. The first method yields bulk sensitive spectra. The second is sensitive to the liquid in the double layer because of the short mean free path of electrons (~1 nm).

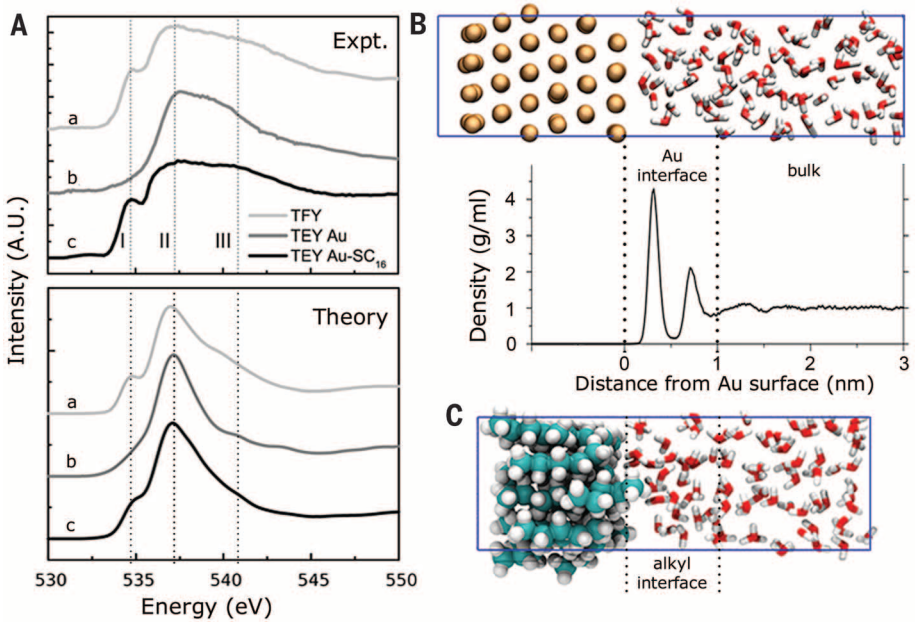


**Fig. 2. Water/gold interface at open circuit potential.** (**A**) Experimental and theoretical XAS at the O K-edge of water near the gold electrode, measured under open circuit in the liquid flow cell (Fig. 1). Curves marked (a) correspond to the total fluorescence yield (TFY) spectrum and calculated XAS spectrum for bulk water. Curves marked (b) correspond to the total electron yield (TEY) spectrum and calculated XAS spectrum for the interfacial water molecules next to the gold electrode. Curves marked (c) correspond to the TEY spectrum of water after covering the gold surface with a hexadecanethiol ($C_{16}SH$) monolayer and calculated XAS spectrum for interfacial water molecules next to an alkyl surface, respectively. Snapshots from AIMD simulations of (**B**) Au-water, with associated mass density as a function of distance from the surface, and (**C**) $C_{16}SH$–water interface, with the gold atoms omitted in the latter case for computational efficiency. The water column separating the Au electrodes is large enough that the water density fluctuations are smoothed beyond the first few layers. Only half of the water column space is shown.

interface. For example, STM and infrared spectroscopy studies of a nonwetting bilayer film have revealed fully saturated H-bonds at the Au(111) surface (*30*). By contrast, calculations (*31*, *32*) and scanning tunneling microscopy (STM) studies of water on more reactive surfaces, such as Ru and Pd, indicate the formation of hexagonal structures in the first layer of water, where the molecules lie flat on the surface and bind to the metal through the oxygen lone-pair electrons in geometries that maximize the number of hydrogen bonds to other water molecules (*33*).

To verify that the suppression of the pre-edge in the XAS of interfacial water molecules is caused by coupling to the gold electronic structure, we performed an experiment with the gold surface covered with a monolayer of hexadecanethiol ($C_{16}H_{33}SH$) that rendered the surface hydrophobic. AFM images of this surface revealed the absence of defects exposing the gold substrate within the ~1-nm resolution of the technique (*34*). Our AIMD calculations revealed an increase in the SD and ND populations at the interface (42 and 9% respectively, relative to the bulk (22 and 1%, respectively; Fig. 3, A and C). The large population of SD and ND species from our AIMD simulations is consistent with vibrational SFG results by Shen *et al.*, which showed a substantial amount of dangling hydrogen bonds in water at the alkyl-water interface (*7*). The TEY XAS result (curve c in Fig. 2) showed a prominent peak at 535 eV characteristic of liquid water, whereas the TFY XAS remained the same as in the case of bare Au/water. Our calculations indicate that the low-energy core-excited states of the interfacial SD and ND molecules are no longer coupled with the (now distant) gold and are highly localized on the excited molecules, therefore producing the pre-edge absorption feature seen in the bulk.

Because water molecules have a strong dipole moment, it is expected that they will respond to external electrical fields (*35*). Infrared spectroscopy results have indeed shown a bias-dependent orientation of the molecules by monitoring the intensity of O-H and H-O-H vibrational modes as a function of applied bias (*5*). We thus investigated the influence of electric fields on the interfacial water structure in the EDL. To separate the large Faradaic current reaching the sample from the electrolyte (typically microamperere or hundreds of nanoamperere) and the much smaller TEY XAS current (500 pA to 10 nA), we modulated the incoming x-ray beam with a piezo-actuated chopper (shown schematically in fig. S5) (*20*) and measured the modulated TEY current with a lock-in amplifier. In this manner, XAS spectra were obtained at bias voltages ranging from –60 to 300 mV relative to a Ag pseudo-reference electrode (*20*).

The results are shown in Fig. 4. At positive bias, the pre-edge peak in the O K-edge spectrum

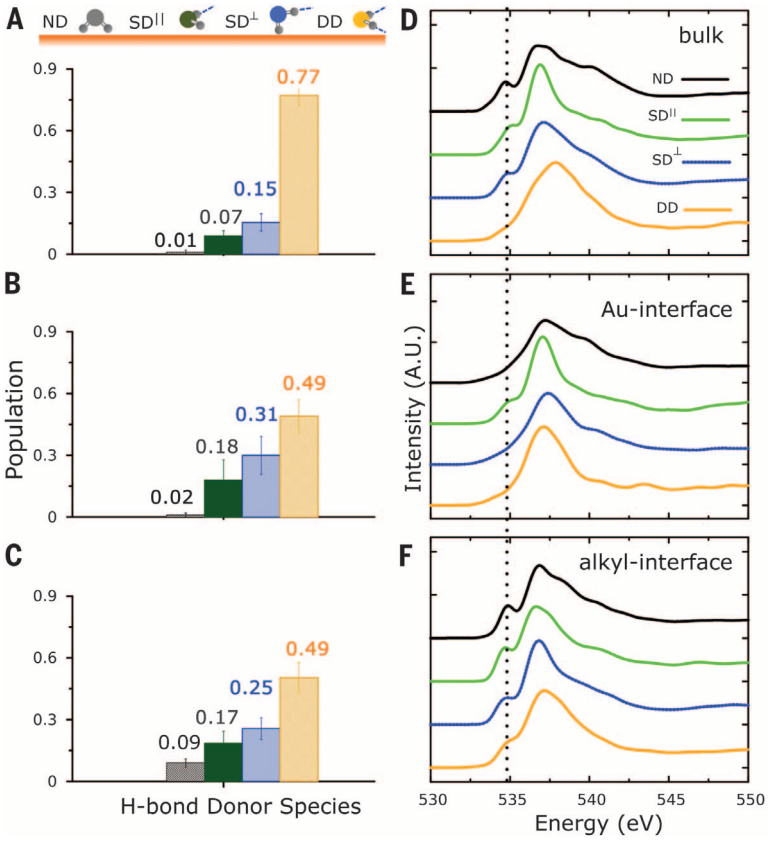


**Fig. 3. Populations of water molecules of various orientations obtained from AIMD simulations and calculated XAS.** In AIMD simulation, the water molecules were sampled: (**A**) from bulk water, (**B**) at the Au interface, and (**C**) at the alkyl interface. Schematics of the nondonor (ND, black), single-donor parallel and perpendicular to the surface ($SD^{||}$ green, $SD^{\perp}$ blue), and double-donor (DD, yellow) molecules shown at the top. Same color code is used for the calculated XAS from water molecules sampled from bulk water (**D**), at the Au interface (**E**), and at the alkyl interface (**F**).

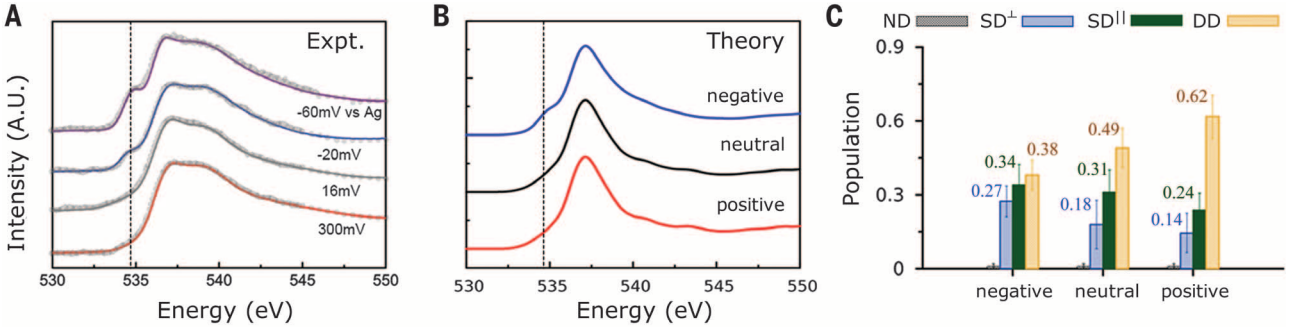


**Fig. 4. The potential-dependence of water XAS spectra and calculated hydrogen-bonding populations.** (**A**) TEY O K-edge XAS of water collected at the Au electrode under different potentials versus a Ag quasi-reference electrode. The point of zero charge (PZC) is found to be at 80 mV (fig. S6). At positive bias, the pre-edge peak at 535 eV characteristic of dangling H-bonds is negligible, whereas it is prominent under negative bias. (**B**) Calculated O K-edge XAS. The pre-edge peak at negative bias is the result of an increase in the population of single-donor ($SD^{||}$) molecules lying parallel to the surface with core-excited states that are decoupled from the gold. (**C**) Population of H-bonded water molecules as a function of the Au surface charge state.

was negligible, as in the case without applied bias, but under negative bias, the pre-edge feature became prominent. Because no electrochemical reactions or ion adsorption take place at these bias voltages (fig. S2) (*20*), a simple interpretation of the observations is that under negative bias, the electric field favors an orientation of the water molecules with their H atoms toward the gold surface, which increases the number of dangling hydrogen bonds. This hypothesis was confirmed by our AIMD simulations, which show an enhanced DD population at positive bias and an enhanced SD population at negative bias (Fig. 4). Indeed, at negative bias, the change in the orientation of the water molecules greatly disrupts the hydrogen bonding network in the interfacial layer (fig. S4) (*20*). This gives rise to an increased $SD^{||}$ population that causes a prominent pre-edge feature in the XAS.

Because XAS is element-specific, our experimental method opens the way for further studies of the structure and chemistry of solvent and solute species in the interfacial layers close to an electrode (~1 nm), and in the presence of electric fields. The complexity of the interfacial molecular rearrangements underscores the need for accurate and efficient first-principles calculations to aid interpretation and, as in the present case, to uncover previously unknown physics related to the strong coupling of x-ray excited states to surface electronic structure. This combined experimental and theoretical approach is essential for a fundamental understanding of electrochemical reactions, with applications to electrocatalysis, photochemistry, and energy storage, among others.

## REFERENCES AND NOTES


1. A. J. Bard, L. R. Faulkner, *Electrochemical Methods: Fundamentals and Applications* (Wiley, New York, 1980).
2. G. Cicero, J. C. Grossman, E. Schwegler, F. Gygi, G. Galli, *J. Am. Chem. Soc.* **130**, 1871–1878 (2008).
3. D. Chandler, *Nature* **437**, 640–647 (2005).
4. P. Fenter *et al.*, *J. Colloid Interface Sci.* **225**, 154–165 (2000).
5. K. Ataka, T. Yotsuyanagi, M. Osawa, *J. Phys. Chem.* **100**, 10664–10672 (1996).
6. M. Fleischmann, P. J. Hendra, I. R. Hill, M. E. Pemble, *J. Electroanal. Chem.* **117**, 243–255 (1981).
7. Y. R. Shen, V. Ostroverkhov, *Chem. Rev.* **106**, 1140–1154 (2006).
8. L. Zhang, C. Tian, G. A. Waychunas, Y. R. Shen, *J. Am. Chem. Soc.* **130**, 7686–7694 (2008).
9. V. Ostroverkhov, G. A. Waychunas, Y. R. Shen, *Phys. Rev. Lett.* **94**, 046102 (2005).
10. J. Sung, L. Zhang, C. Tian, Y. R. Shen, G. A. Waychunas, *J. Phys. Chem. C* **115**, 13887–13893 (2011).
11. A. Nilsson *et al.*, *J. Electron Spectrosc. Relat. Phenom.* **177**, 99–129 (2010).
12. H. Bluhm, D. F. Ogletree, C. S. Fadley, Z. Hussain, M. Salmeron, *J. Phys. Condens. Matter* **14**, L227–L233 (2002).
13. A. Nilsson, L. G. M. Pettersson, *Surf. Sci. Rep.* **55**, 49–167 (2004).
14. J.-H. Guo *et al.*, *Phys. Rev. Lett.* **89**, 137402 (2002).
15. O. Fuchs *et al.*, *Nucl. Instruments Methods A* **585**, 172–177 (2008).
16. T. Tokushima *et al.*, *J. Chem. Phys.* **136**, 044517 (2012).
17. J.-H. Guo *et al.*, *Phys. Rev. Lett.* **91**, 157401 (2003).
18. P. Jiang *et al.*, *Electrochem. Commun.* **12**, 820–822 (2010).
19. A. Braun *et al.*, *J. Phys. Chem. C* **116**, 16870–16875 (2012).
20. See supplementary materials in *Science* Online.
21. S. Ghosal *et al.*, *Science* **307**, 563–566 (2005).
22. M. A. Brown, M. Faubel, B. Winter, *Annu. Rep. Prog. Chem. Sect. C* **105**, 174 (2009).
23. D. Prendergast, G. Galli, *Phys. Rev. Lett.* **96**, 215502 (2006).
24. U. Bergmann *et al.*, *Phys. Rev. B* **66**, 092107 (2002).
25. A. H. England *et al.*, *Chem. Phys. Lett.* **514**, 187–195 (2011).
26. W. S. Drisdell *et al.*, *J. Am. Chem. Soc.* **135**, 18183–18190 (2013).
27. P. Wernet *et al.*, *Science* **304**, 995–999 (2004).
28. G. Cicero, A. Calzolari, S. Corni, A. Catellani, *J. Phys. Chem. Lett.* **2**, 2582–2586 (2011).
29. R. Nadler, J. F. Sanz, *J. Chem. Phys.* **137**, 114709 (2012).
30. D. Stacchiola *et al.*, *J. Phys. Chem. C* **113**, 15102–15105 (2009).
31. P. J. Feibelman, *Science* **295**, 99–102 (2002).
32. A. Michaelides, A. Alavi, D. A. King, *J. Am. Chem. Soc.* **125**, 2746–2755 (2003).
33. M. Tatarkhanov *et al.*, *J. Am. Chem. Soc.* **131**, 18425–18434 (2009).
34. G. Liu, M. Salmeron, *Langmuir* **10**, 367–370 (1994).
35. M. F. Toney *et al.*, *Nature* **368**, 444–446 (1994).


## ACKNOWLEDGMENTS

This work was supported by the Office of Basic Energy Sciences (BES), Division of Materials Sciences and Engineering, of the U.S. Department of Energy (DOE) under contract no. DE-AC02-05CH11231 (through the Chemical and Mechanical Properties of Surfaces, Interfaces and Nanostructures program). J.-J.V.-V. acknowledges financial support from the Alexander von Humboldt Foundation, Germany. C.H.W. acknowledges the Advanced Light Source (ALS) Doctoral Fellowship in Residence. Theory and simulations by T.A.P., L.F.W., and D.P. were supported by the Joint Center for Energy Storage Research, an Energy Innovation Hub funded by the U.S. DOE and facilitated by a user project at the Molecular Foundry. Computations were performed with the computing resources of the National Energy Research Scientific Computing Center (NERSC). The ALS and Molecular Foundry (supported by DOE-BES) and NERSC (supported by DOE–Advanced Scientific Computing Research) are DOE Office of Science User Facilities, supported by the DOE Office of Science under contract no. DE- AC02-05CH11231. We thank C.-H. Chuang, B.-Y. Wang, D. Zhang, X. Feng, and M. W. West for support at the beamline. We also thank J. Zhang for help with AFM imaging and C. Das Pemmaraju, C. Schwartz, P. Ross, J. Colchero, G. Thornton, H. Fang, and S. Harris for useful discussions.

## SUPPLEMENTARY MATERIALS

www.sciencemag.org/content/346/6211/831/suppl/DC1
Methods
Figs. S1 to S6
References (*36*–*65*)

31 July 2014; accepted 9 October 2014
Published online 23 October 2014;
10.1126/science.1259437

STRONG BASES

# Directed ortho-meta′- and meta-meta′-dimetalations: A template base approach to deprotonation

**Antonio J. Martínez-Martínez, Alan R. Kennedy, Robert E. Mulvey,* Charles T. O'Hara***

**The regioselectivity of deprotonation reactions between arene substrates and basic metalating agents is usually governed by the electronic and/or coordinative characteristics of a directing group attached to the benzene ring. Generally, the reaction takes place in the ortho position, adjacent to the substituent. Here, we introduce a protocol by which the metalating agent, a disodium-monomagnesium alkyl-amide, forms a template that extends regioselectivity to more distant arene sites. Depending on the nature of the directing group, ortho-meta′ or meta-meta′ dimetalation is observed, in the latter case breaking the dogma of ortho metalation. This concept is elaborated through the characterization of both organometallic intermediates and electrophilically quenched products.**

One of the most widely applied chemical reactions is metalation (*1*, *2*), in which an inert carbon-hydrogen (C-H) bond is transformed to a more reactive carbon-metal (C-M) bond by a metalating agent. The fundamental importance and vast scope of metalation arise from the ubiquity of the C-H bond, which is one of the most abundant bonds found in nature and provides a rich sustainable entry point for the synthesis of aromatic chemicals, natural products, and organic-based materials. However, this abundance of C-H bonds poses a formidable challenge to synthetic chemists: How can metalation reactions be made regioselective—that is, to deprotonate specific C-H bonds without reacting with other C-H bonds in the same molecule? One answer arrived in "directed ortho-metalation" (DoM) (*3*–*6*), the seminal concept to date in metalation chemistry. First introduced independently by Gilman (*7*) and Wittig (*8*), and then greatly extended by Beak (*9*), Mortier (*10*), Hoppe (*11*, *12*), and Snieckus (*13*, *14*), among others, DoM relies primarily on the substitution within the aromatic substrate undergoing the C-H to C-M transformation. To induce the DoM reaction, this substrate must contain a directing metalation group (DG) that can activate an adjacent (ortho) C-H bond toward metalation either by providing the incoming Lewis acidic metalating agent with a Lewis basic docking site (coordination effect) and/or weakening this bond through electron-withdrawing inductive properties (electronic effect) (Fig. 1). Depending on their relative coordinating and electron-withdrawing ability, DGs can be weak, moderate, or strong ortho-directors.

In general, the DoM concept applies irrespective of which metalating agent is used, whether it be an organolithium reagent or one of the new wave of bimetallic formulations [typified

WestCHEM, Department of Pure and Applied Chemistry, University of Strathclyde, Glasgow G1 1XL, UK.
***Corresponding author. E-mail: r.e.mulvey@strath.ac.uk (R.E.M.); charlie.ohara@strath.ac.uk (C.T.O)**